Journal of Power Sources 213 (2012) 100–105

Contents lists available at SciVerse ScienceDirect

Journal of Power Sources

journal homepage: www.elsevier.com/locate/jpowsour

Synthesis and characterization of high power $LiFePO_4$/C nano-plate thin films

Nan Zhou [a,b], Yanyi Liu [a], Jiangang Li [a,c], Evan Uchaker [a], Suqin Liu [b], Kelong Huang [b], Guozhong Cao [a,*]

[a] Department of Materials Science and Engineering, University of Washington, Seattle, WA 98195, USA
[b] College of Chemistry and Chemical Engineering, Central South University, Changsha, Hunan 410083, China
[c] Department of Applied Chemistry, Beijing Institute of Petrochemical Technology, Beijing 102617, China

ARTICLE INFO

Article history:
Received 15 February 2012
Received in revised form
9 April 2012
Accepted 10 April 2012
Available online 16 April 2012

Keywords:
Thin film cathode
Lithium iron phosphate
Lithium ion battery
Solvothermal growth
Nano-carbon coating

ABSTRACT

Tunable $LiFePO_4$/C thin films demonstrating high power were fabricated by drop-casting a $LiFePO_4$ nano-plate/sucrose suspension on titanium foil, followed by pyrolysis at 600 °C for 3 h in nitrogen. The thickness, carbon content, and morphology of the $LiFePO_4$/C film cathode can be adjusted by changing the amount of drop-cast, sucrose solution concentration and $LiFePO_4$ raw material. For this work, well-crystallized $LiFePO_4$ nano-plates synthesized via solvothermal route were used to prepare high power $LiFePO_4$/C thin films. The resultant binder-free films consisted of well-packed $LiFePO_4$ nano-plates coated with nano-carbon, a result of sucrose pyrolysis, and were directly assembled into cells for testing. The $LiFePO_4$/C nano-composite film cathode delivered a lithium ion intercalation capacity of 162 mAh g^{-1} and 90 mAh g^{-1} at current density of 170 mA g^{-1} (1 C) and 1.7 A g^{-1} (10 C), respectively, while demonstrating excellent cyclic stability.

1. Introduction

Thin film lithium ion batteries have been developed over recent years to accommodate our increasingly mobile and technology driven society [1]. These batteries exhibit the same voltage and current as the traditional rechargeable lithium ion batteries; however, their reduced dimensions make possible their use in novel applications such as implantable medical devices with reduced weight and volume. Cathode materials for thin film lithium ion batteries are typically metal oxides [2–4] that have been directly deposited as a film using various methods such as pulsed laser deposition (PLD) [5,6], bias sputtering [7], radio frequency (rf) magnetron sputtering [8–10], electrostatic spray deposition (ESD) [11,12], and sol-gel spin coating [13–16].

Lithium iron phosphate ($LiFePO_4$ or LFP) has attracted much attention in both the research and industrial communities for its high theoretical capacity of 170 mAh g^{-1}, flat discharge voltage at ~3.4 V, abundance of raw materials leading to low cost, and excellent thermal and chemical stability [17,18] since it was first reported in 1997 [19]. Though traditional cathode materials such as $LiCoO_2$, $LiNiO_2$, *etc.* have been successfully commercialized and continue to play an indispensable role in today's Li-ion batteries, $LiFePO_4$ is considered to be one of the most promising cathode candidates for advanced lithium ion batteries, which are used in high energy and high power systems [20]. However, the wide-spread commercialization of $LiFePO_4$ has been hindered due to its low electrical conductivity, which also limits its application in high power devices [21–23]. Thus, the development of $LiFePO_4$ has been widely investigated over the past 10 years, from the synthesis process to the electrochemical conductivity; with recent research on $LiFePO_4$ now taking focus on its application in thin film lithium ion battery. $LiFePO_4$ thin film was actually fabricated as early as 2004 [6], but most of the early works were focused on the kinetics of the lithium ion insertion/deinsertion process of carbon and binder-free lithium iron phosphate [24]. Later on, conductive coating was introduced to improve the electrochemical performance of $LiFePO_4$ thin films [3,25,26]. However, the investigation of tunable $LiFePO_4$ thin films with high power is still lacking.

Recently, Liu et al. fabricated uniform and crack-free nano-structured $LiFePO_4$/carbon nano-composite film cathodes by spreading $LiFePO_4$/ascorbic acid sol on a Pt coated Si wafer, following with ambient drying overnight and annealing/pyrolysis at elevated temperature in nitrogen [27]. This film demonstrated excellent Li-ion intercalation properties due to the relatively poor crystallinity which provided a less packed structure for easier accommodation of lithium ions. Surface defects and conductive nano-coating effectively improved the charge-transfer property and phase transition during Li-ion intercalation/deintercalation. In this work, $LiFePO_4$/C nano-composite high energy thin films were successfully fabricated while controlling the thickness, carbon content and morphology. These tunable, binder-free and high power $LiFePO_4$/C thin films were

* Corresponding author. Tel.: +1 206 616 9084; fax: +1 206 543 3100.
E-mail address: gzcao@u.washington.edu (G. Cao).

0378-7753/$ – see front matter © 2012 Elsevier B.V. All rights reserved.
doi:10.1016/j.jpowsour.2012.04.022

prepared by adding well-crystallized solvothermally processed $LiFePO_4$ nano-plates into a sucrose-water solution and then drop-casting the suspension on titanium foil followed by annealing/pyrolysis in a nitrogen environment at elevated temperatures. The resulting films showed excellent storage performance at high charge and discharge currents while demonstrating good cyclic stability.

2. Experimental

2.1. Synthesis of $LiFePO_4$ nano-plates by solvothermal route

The $LiFePO_4$ powder was prepared via solvothermal route according to literature [28]. Lithium dihydrogen phosphate LiH_2PO_4 (≥99.0%, Aesar) and Iron (II) oxalate dihydrate $FeC_2O_4 \cdot 2H_2O$ (≥99.0%, Aldrich) were separately dissolved in ethylene glycol (EG) to form 0.1 mol L^{-1} solutions. The solutions were then mixed together and ultrasonicated for 1 h. The overall molar ratio of Li:Fe:P was 1:1:1. The obtained mixture was transferred into a 30 ml PTFE lined stainless steel autoclave and heated at 200 °C for 8 h. The product was then cooled to room temperature and isolated with ethanol and de-ionized water several times. Pure light gray $LiFePO_4$ powder, or LFP powder, was obtained after drying at 60 °C overnight.

2.2. Fabrication of $LiFePO_4$/C nano-plate films

First, 10 mg of sucrose (EMD) was dissolved in 5 ml of de-ionized water to which 4 mg of the aforementioned $LiFePO_4$ powder was added and dispersed in solution. The suspension was ultra-sonicated for 2 h to form a homogeneous dispersion. The $LiFePO_4$/C nano-plate composite films were prepared by drop-casting 25 μl, 50 μl, and 75 μl of the suspension onto titanium foil which were then placed in a petri dish and covered with edge perforated plastic film. After being dried under ambient conditions for 72 h, the samples were annealed at 600 °C in N_2 for 3 h (herein denoted as LFP/C film). The film obtained from the 50 μl of suspension drop had a geometric area of approximately 0.2 cm^2 and was used for further analysis.

2.3. Structural characterization and property measurements

X-Ray Diffraction (XRD) patterns were obtained using a D8 Bruker X-ray diffractometer equipped with Cu-Kα radiation. The accelerating voltage and current were 40 kV and 40 mA, respectively. A scan speed of 0.02° per second was used. Scanning electron microscopy (SEM) images and energy-dispersive X-ray spectroscopy (EDAX) analysis were taken with a JEOL JSM-7000F field emission scanning electron microscope operated at 10 kV and 10 mA.

For energy storage studies, the obtained $LiFePO_4$/C nano-plate composite films were assembled directly into a two-electrode Swagelok-type cell in an Argon-filled glove box. Lithium metal foil, 1 M $LiPF_6$ in ethylene carbonate (EC)/dimethyl carbonate (DMC) (1:1, in weight) and Celgard 2400 membrane were used as counter electrode, electrolyte and separator respectively. Charge-discharge cycling tests of the assembled cells under constant current mode were carried out using a computer controlled electrochemical analyzer (Model BT2000, Arbin Instruments, USA) in the voltage range of 2.5–4.2 V (*vs.* Li^+/Li).

3. Results and discussion

Fig. 1(a–c) shows side view SEM images of the three thin films obtained from drop-casting 25 μl, 50 μl, 75 μl of the preliminary suspension on titanium foil following with annealing and pyrolysis treatment. The thicknesses of the three films are approximately 2 μm, 2.5 μm and 3 μm, respectively; and the film thickness increases about 0.5 μm with each subsequent addition of 25 μl of the dispersion. This demonstrates that the thickness of the LFP/C thin film can be controlled by regulating the amount of the

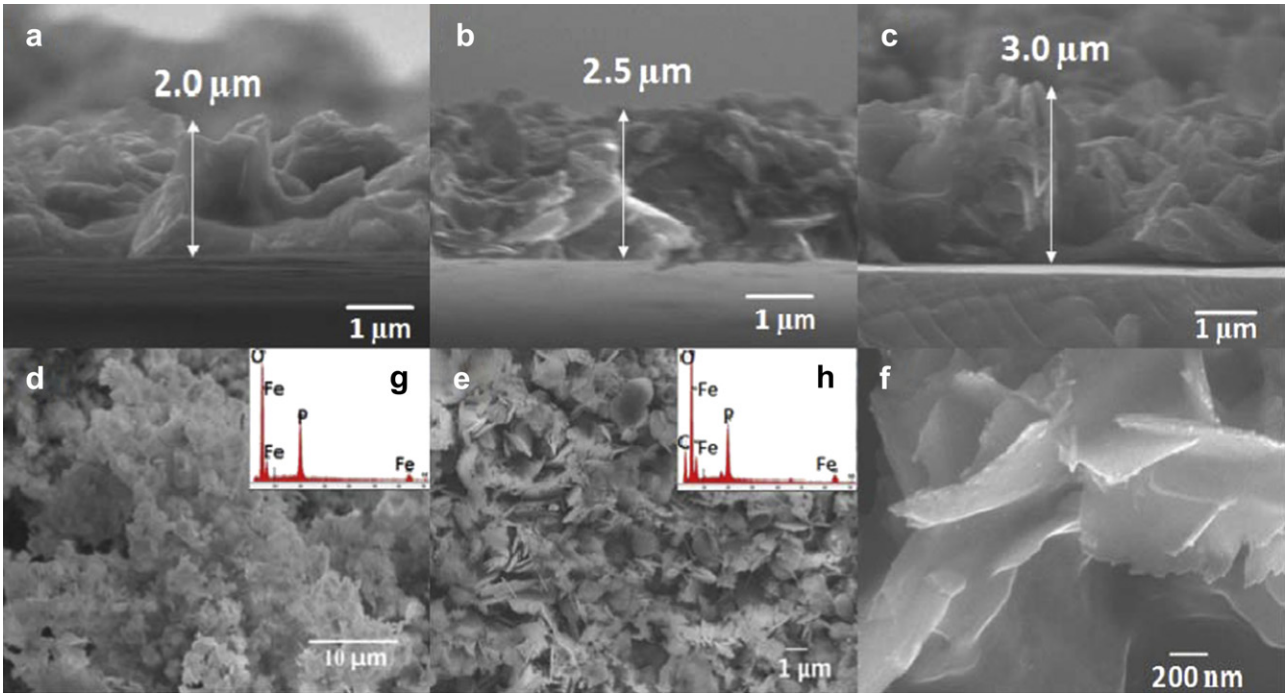

Fig. 1. SEM micrographs of:(a) side view of the 25 μl LFP/C film, (b) side view of the 50 μl LFP/C film, (c) side view of the 75 μl LFP/C film, (d) LFP powder, (e) overall morphology of the 50 μl LFP/C film, (f) high-magnification image of the 50 μl LFP/C film; and EDAX analysis (inset) of (g) LFP powder, (h) the 50 μl LFP/C film.

suspension used for drop-casting. SEM images also revealed the LFP/C thin film is highly porous rather than dense, which is usually obtained with other deposition methods [29,30]. The large surface area and high porosity of the cathode would permit easy penetration of electrolyte and rapid lithium ion intercalation/deinterclation. For the sake of clarity, further discussion will only focus on the results of the LFP/C thin film obtained from the 50 μl drop-cast suspension. SEM images in Fig. 1(d–f) show the morphology of the LFP powder and LFP/C composite film. The LFP crystals have an irregular plate-like shape, suggesting the growth conditions took place away from thermodynamic equilibrium or were at least partly diffusion controlled. The average thickness of the nano-plates is relatively uniform at approximately 30 nm. It is well known that one of the advantages of using nano-sized materials is the corresponding high specific surface area that eases the interfacial intercalation/deintercalation reaction and provides rapid and easy ion/electron transport; however, such high specific surface energy would also lead to particle agglomeration in an attempt to decrease the surface energy. This might explain the clustering of $LiFePO_4$ particles; such agglomeration could retard the diffusion of lithium ions and electron transition from the electrolyte into the active material [31]. Fig. 1(e) and (f) shows that $LiFePO_4$ nano-plates were separated and dispersed homogenously in the film after ultrasonication and heat treatment, which lead to the high porosity of the film and would accelerate electrolyte penetration and Li^+ ion transition. The element constituents of the LFP powder and LFP/C film were analyzed by means of EDAX and the results, shown in the inset of Fig. 1(g) and (h), correspond well to $LiFePO_4$; however, there was a large difference in the carbon content of the samples, as confirmed by the presence of carbon resulting from sucrose pyrolysis in the LFP/C film. Although carbon spheres or micro-beads from sucrose pyrolysis have been widely reported in literature [32], 600 °C might be too low to form such carbon spheres or micro-beads, and instead the carbon forms a homogeneous and uniformly dispersed coating on the surface of the $LiFePO_4$ nano-plates. The homogeneous dispersion of carbon throughout the LFP/C film forms a network connecting individual $LiFePO_4$ nano-plates, effectively providing conductive pathways and improving the electrochemical performance of the $LiFePO_4$/C composite film [33]. Surface carbon could also be present as surface defects that serve as nucleation sites to promote phase transition [34,35]. Another advantage realized by the homogeneous carbon coating is that the phase transition during Li-ion intercalation/deintercalation can be greatly enhanced because of the lower nucleation activation energy offered by the $LiFePO_4$–C-electrolyte three-phase interface [36–39].

Fig. 2 summarizes and compares the XRD patterns of the solvothermal-grown LFP powder and the LFP/C composite thin film; also included in Fig. 2 is the standard XRD pattern for $LiFePO_4$. Both XRD patterns of the LFP powder and LFP/C film exhibit the same major peaks and correspond well with crystallized orthorhombic $LiFePO_4$ (PDF#98-000-0443) without any detectable parasitic phases. The difference in intensity between the two patterns can be attributed to the increase in degree of crystallinity of the $LiFePO_4$ raw material in the LFP/C film after annealing at 600 °C for 3 h. The absence of diffraction peaks corresponding to crystalline carbon (graphite) suggests that the carbon generated from sucrose pyrolysis is amorphous carbon, a result that is commonly observed in literature for other carbon coating materials [40,41]. The presence of amorphous carbon has no detectable influence on the crystal structure of $LiFePO_4$. The lattice parameters of the LFP powder and LFP/C thin film as estimated from the XRD results are: 1) a – 10.3398 Å, b – 5.991 Å, c – 4.6949 Å for the LFP powder; and 2) a – 10.3345 Å, b – 6.0075 Å, c – 4.8645 Å for the LFP/C film, respectively, all of which agree well with those values

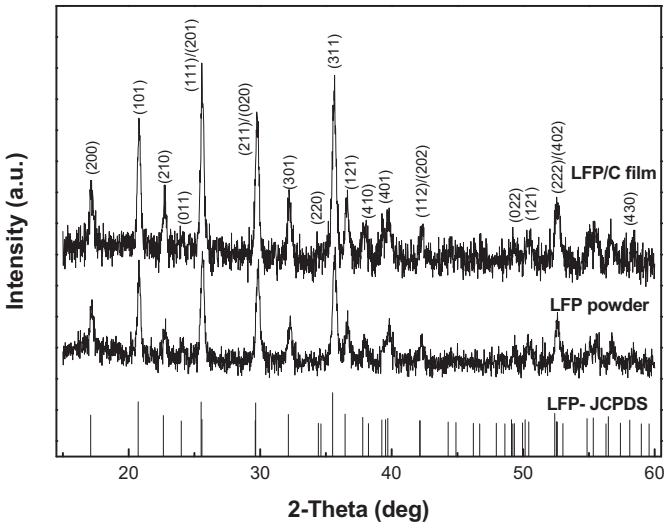

Fig. 2. X-Ray Diffraction patterns of the LFP/C film, LFP powder, and LFP-JCPDS standard.

reported in literature [18]. Kanumasa et al. [42] suggested that the needle-shaped crystal morphology should be present if the intensity of the (200) peak is greater than that of the (020) peak, whereas platelet-type structures would be seen if the intensity of the (020) peak is higher than the (200) peak. The patterns in Fig. 2 exhibit a higher intensity for the (020) peak than the (200) peak, suggesting that the synthesized $LiFePO_4$ should possess platelet like morphology, which is corroborated by the SEM results. Such morphology would have a good impact on lithium intercalation/deintercalation as it favors lithium ion diffusion [28].

Saravanan et al. [28] suggested that LFP nano-plates obtained from solvothermal synthesis are single crystalline, with the *b*-axis oriented along the thinnest direction while the large face of the plate lies within the *ac* plane. Independent *ab-initio* [43] calculations and atomistic simulations [44] have suggested that Li ions would diffuse preferably along the *b*-axis rather than along the *a*- or *c*-axes in crystals with orthorhombic space group *Pnma* [31]. The solvothermal synthesized LFP nano-plates, with reduced thickness along the *b*-axis, should therefore show enhancement of Li^+ insertion and extraction. Thus, the solvothermal-grown $LiFePO_4$ nano-plates were mixed with a sucrose-water solution to be the bulk material for fabrication of high power LFP/C thin films. It is worth noting that besides $LiFePO_4$ nano-plates, other active materials such as $LiMnPO_4$, $LiCoO_2$, and $LiMn_2O_4$, *etc.*, with different shapes such as spheres, particles, or three-dimensional structures of nano- or even micro-meter size can also be added into the sucrose solution followed with the annealing treatment to form cathodic films for lithium ion thin film batteries. This deposition method greatly reduced agglomeration of the bulk material caused by the small particle size, thus preventing any potential drawbacks of decreasing the surface area while the homogeneous nano-carbon coating derived from sucrose pyrolysis enhances the electrochemical performance.

In conventional electrode processing, the active materials have to be pretreated by adding 10–20 wt% of conductive additives (i.e. carbon black) and binder (i.e. PVDF) before cell assembly, often leading to inadequate contact between particles and thus impeding the lithium ions from diffusing effectively in certain areas. Low binder content would lead to structural instability of the cathode over a lifetime of charge-discharge cycles, but higher binder content would obstruct the electron transfer as most binders are insulators. The use of additives and binders also contributes significantly to the

cathode mass, resulting in lowered specific energy and power density which is calculated based on the mass of the entire electrode. In contrast to conventional processing, the nano-composite thin film cathode developed in this study does not require any insulative binder. The carbon derived from sucrose pysolysis ensures the $LiFePO_4$ nano-plates are homogeneously dispersed and adhere well onto the Ti substrate. The carbon functions as both conductive network and binding agent.

The processes of treating the $LiFePO_4$ clustered powder to form the LFP/C thin films are summarized. First, sucrose was dissolved in water to form a sucrose-water solution, followed by adding the clustered $LiFePO_4$ nano-plate powder. Then, the suspension was ultrasonicated for 2 hours to separate the $LiFePO_4$ nano-plates. The suspension was subsequently drop-cast on titanium foil and covered with plastic film and dried under ambient environment to form homogeneous precursor films. It is worth noting that the remaining sucrose from the solution played an important role in preventing the $LiFePO_4$ nano-plates from agglomerating with each other. The film was then annealed in nitrogen to pyrolyze the sucrose into carbon, so as to obtain $LiFePO_4$ nano-plates thin films uniformly coated with carbon webbing.

The LFP/C composite thin films were assembled directly into a two-electrode Swagelok-type cell to analyze the electrochemical properties. Only the mass of $LiFePO_4$ was included when calculating the specific capacity of the LFP/C film since the capacity contribution of the nano-carbon coating was negligible between the voltage limits of 2.5 and 4.2 V in our examination. Fig. 3 shows the first three cycles of the lithium ion charge–discharge process in the LFP/C composite film at a rate of 1 C. The film exhibited a storage capacity of 162 mAh g^{-1} with a voltage plateau at about 3.35 V *vs.* Li^+/Li, close to the theoretical value (170 mAh g^{-1}) of $LiFePO_4$ and exceeding most storage values under the same charge rate reported in literature [45]. The irreversible capacity loss between the first charge and discharge reaction is about 6.5 mAh g^{-1}, and the Columbic efficiency (calculated from discharge capacity/charge capacity) is 96%. The polarization between the charge and the discharge plateaus was quickly reduced and became steady as the cycles increased, which could be attributed mainly to the slow penetration of the electrolyte through the carbon coating and into the particles' interior, progressively forming an active surface area of $LiFePO_4$ [40]. A shorter plateau and longer sloped region appear in the charge and discharge curves of the LFP/C thin film when compared with conventional $LiFePO_4$ materials, a similar phenomenon has previously been reported in literature [46]. One of

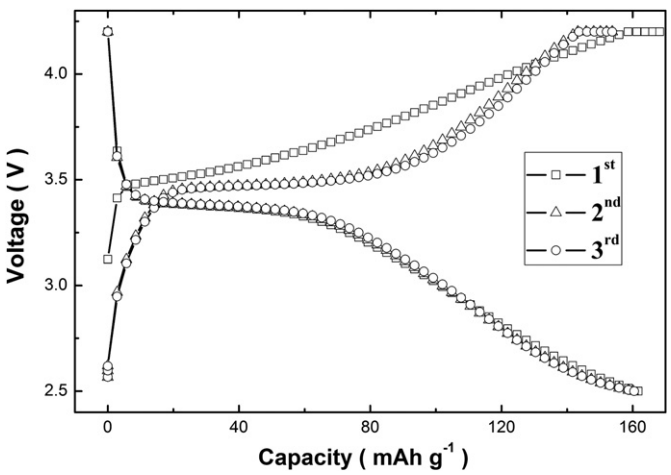

Fig. 3. Initial three cycles of charge/discharge performance of the LFP/C composite film at 1 C rate between 2.5 and 4.2 V (*vs.* Li^+/Li).

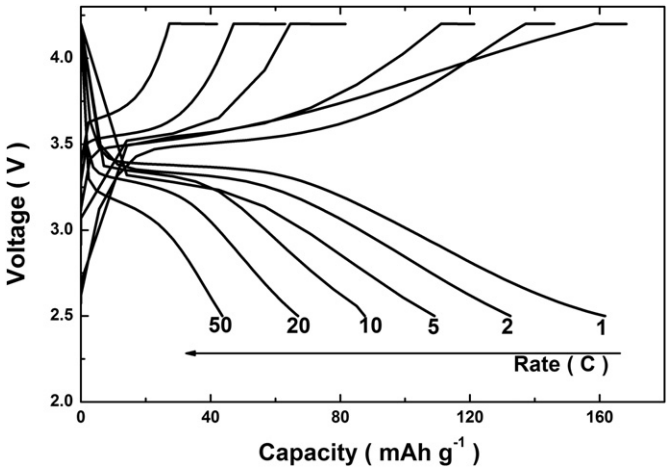

Fig. 4. Initial galvanostatic charge/discharge performance of the LFP/C composite film at different rates between 2.5 and 4.2 V (*vs.* Li^+/Li).

the two possible explanations for this trend in the charge/discharge profile is the formation of a single-phase solid solution, which is related to particle size. Meetong et al. [47] tested three different sized $LiFePO_4$ particles and found that the solid solution stabilized only when the particle size was below 45 nm, which was further confirmed by Gibot and his group [48]. In the present work, the nano-plates obtained from solvothermal growth are ~400 nm in length, much larger than this critical size; it is unlikely a solid solution would form. Another point to consider is the slope represents the capacitive behavior of the surface or interfacial storage of lithium ions [49]. Both lithium ion intercalation and surface capacitive adsorption contributed to the total storage capacitance of the material [50]. This kind of surface behavior has been termed the pseudocapacitive effect and has recently been found in many high surface area and nano-structure materials [51–53].

The initial charge–discharge curves at various current rates for the LFP/C composite film are shown in Fig. 4. It can be seen that although the capacity inevitably decreased with increasing current density, such nano-composite thin film cathodes delivered initial discharge capacities of 132 mAh g^{-1}, 109 mAh g^{-1}, 90 mAh g^{-1}, and 67 mAh g^{-1} at rates of 2 C, 5 C, 10 C, and 20 C, respectively.

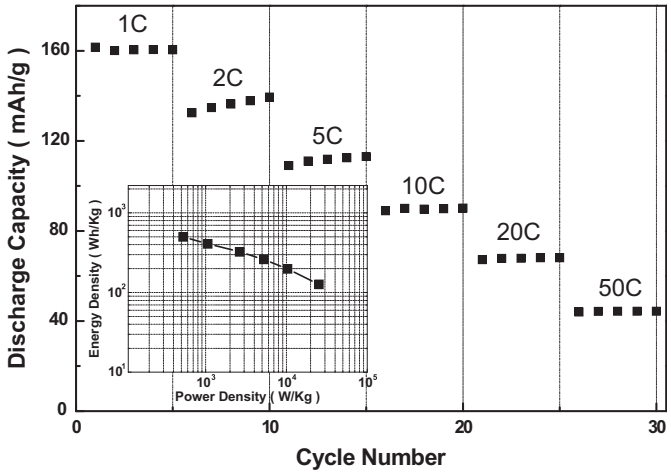

Fig. 5. Energy storage performance of the LFP/C composite film at different rates between 2.5 and 4.2 V (*vs.* Li^+/Li) and insertion: Regone plot for the LFP/C composite film.

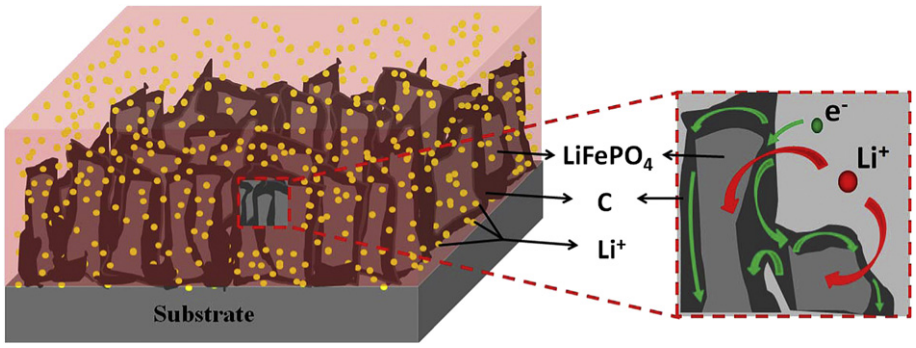

Fig. 6. Schematic of the micro-structure and nano-structure of the LFP/C thin film.

A discharge capacity of 44 mAh g^{-1} was even recorded at the high rate of 50 C. It is worth noting that even at such a high current density, the voltage plateau of the discharge curve still remained above 3.1 V. The exceptional Li-ion intercalation performance at the high rate condition could be attributed to the high phase purity, large surface area and short *b*-axis diffusion path of the nano-plates, combined with the fine dispersion of the nano-carbon connecting web. The nano-sized plate shape of the $LiFePO_4$ particle coated with conductive carbon and the high porous structure of the thin film: (a) ensures a large surface area of the reaction phase between electrolyte and active material, (b) reduces the diffusion length of the lithium ions and electrons, and (c) improves the conductivity of the cathode as a whole. The combination of these effects permits a fast reaction and quick diffusion processes.

Fig. 5 shows the lithium intercalation capability of the LFP/C thin film during the first five cycles at different rates. The excellent storage performance of the LFP/C thin film at high rates indicate that the cathode films fabricated from the $LiFePO_4$ nano-plates/sucrose suspension would be well suited for high power lithium ion thin film battery. The inset in Fig. 5 shows the power and energy densities of the LFP/C nano-composite film electrode, which demonstrates that this LFP/C thin film has better energy storage performance than conventional $LiFePO_4$/C powder electrodes. Such effects may be due to the short lithium ion transition pathway and well percolated carbon nano-coating of the nano-plate films since the ability of lithium ions to travel across the interface between the electrolyte and active material phases is crucial for ultrafast diffusion [54].

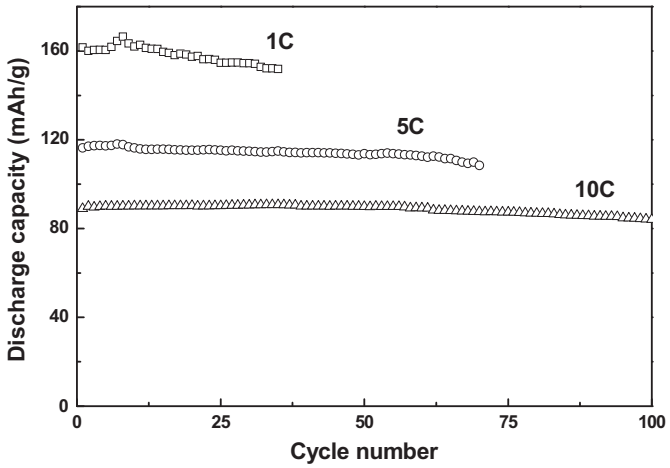

Fig. 7. Cycle performance of the LFP/C composite film at rate of 1 C, 5 C, 10 C between 2.5 and 4.2 V (*vs.* Li^+/Li).

Fig. 6 schematically illustrates the micro- and nano-structure of the LFP/C thin film. The irregular packing of the solvothermal-grown $LiFePO_4$ nano-plates on the substrate induces a highly porous micro-structure within the films, which eases penetration of the electrolyte and fast diffusion of the lithium ions and electrons. In addition, the spacing between each $LiFePO_4$ nano-plate speeds up Li^+ ion intercalation/deintercalation along the *b*-axis in both sides of the nano-plate. Electron transfer is also accelerated by the homogeneous conductive carbon coating and nano-webbing from sucrose pyrolysis.

Fig. 7 shows the long-term cyclic performances of the LFP/C composite film electrode at different rates of 1 C, 5 C, and 10 C. The discharge capacity dropped 6% after 35 cycles at the 1 C rate and retained 93% of the initial discharge capacity at a higher rate of 10 C over 100 cycles. This outstanding stability should be attributed to the porous LFP/C thin film with well-packed nano-meter sized $LiFePO_4$ crystals.

4. Conclusions

Tunable $LiFePO_4$/C nano-plate films are readily fabricated by the dispersion of solvothermally grown $LiFePO_4$ nano-plates in sucrose solution followed by annealing and pyrolysis in nitrogen at 600 °C. The thickness, carbon content, and morphology of the film can be controlled by adjusting the amount of drop-cast, sucrose solution concentration and $LiFePO_4$ raw material. Carbon residue from sucrose pyrolysis disperses the LFP nano-plates and serves as a conductive nano-coating as well as binding agent. High electrochemical performance with an initial discharge capacity of 162 mAh g^{-1} at a rate of 1 C and 90 mAh g^{-1} at a rate of 10 C with good cyclic stability (6% fading after 35 cycles for 1 C rate and 7% fading after 100 cycles for 10 C rate) were observed for the $LiFePO_4$/C nano-composite film cathodes when tested between 2.5–4.2 V (*vs.* Li^+/Li). The excellent electrochemical performance could be ascribed to the high porosity of the films and fine dispersion of the $LiFePO_4$ nano-plates that guarantees large surface area to ensure fast phase penetration between the electrolyte and active material, and a short migration path along the *b*-axis for lithium ion intercalation/deintercalation. Furthermore, the carbon surface defects and conductive nano-coating may effectively improve the charge-transfer properties and phase transition.

Acknowledgment

NZ gratefully acknowledges fellowship from the China Scholarship Council. This research work has been financially supported in part by the National Science Foundation (NSF, CMMI-1030048), Pacific Northwest National Laboratories (PNNL), and the University of Washington TGIF grant.

References

[1] J.L. Li, C. Daniel, D. Wood, Journal of Power Sources 196 (2011) 2452–2460.
[2] J. Ma, Q.Z. Qin, Journal of Power Sources 148 (2005) 66–71.
[3] Z. Lu, H. Cheng, M. Lo, C.Y. Chung, Advanced Functional Materials 17 (2007) 3885–3896.
[4] V. Patil, A. Patil, J.W. Choi, S.J. Yoon, Solid State Sciences 13 (2011) 1232–1234.
[5] Y. Iriyama, M. Yokoyama, C. Yada, S.K. Jeong, I. Yamada, T. Abe, M. Inaba, Z. Ogumi, Electrochemical and Solid State Letters 7 (2004) A340–A342.
[6] F. Sauvage, E. Baudrin, M. Morcrette, J.M. Tarascon, Electrochemical and Solid State Letters 7 (2004) A15–A18.
[7] K.F. Chiu, Journal of the Electrochemical Society 154 (2007) A129–A133.
[8] Y.J. Park, K.S. Ryu, K.M. Kim, N.G. Park, M.G. Kang, S.H. Chang, Solid State Ionics 154 (2002) 229–235.
[9] H.K. Kim, T.Y. Seong, Y.S. Yoon, Electrochemical and Solid State Letters 5 (2002) A252–A255.
[10] J. Xie, N. Imanishi, T. Zhang, A. Hirano, Y. Takeda, O. Yamamoto, Electrochimica Acta 54 (2009) 4631–4637.
[11] C.H. Chen, E.M. Kelder, J. Schoonman, Thin Solid Films 342 (1999) 35–41.
[12] M. Mohamedi, A. Makino, K. Dokko, T. Itoh, I. Uchida, Electrochimica Acta 48 (2002) 79–84.
[13] H. Porthault, F. Le Cras, S. Franger, Journal of Power Sources 195 (2010) 6262–6267.
[14] V. Patil, A. Patil, J.W. Choi, Y.P. Lee, Y.S. Yoon, H.J. Kim, S.J. Yoon, Journal of Electroceramics 23 (2009) 214–218.
[15] Y.J. Park, J.G. Kim, M.K. Kim, H.T. Chung, H.G. Kim, Solid State Ionics 130 (2000) 203–214.
[16] Y.H. Rho, K. Kanamura, T. Umegaki, Journal of the Electrochemical Society 150 (2003) A107–A111.
[17] A.S. Andersson, J.O. Thomas, B. Kalska, L. Haggstrom, Electrochemical and Solid State Letters 3 (2000) 66–68.
[18] S.T. Myung, S. Komaba, N. Hirosaki, H. Yashiro, N. Kumagai, Electrochimica Acta 49 (2004) 4213–4222.
[19] A.K. Padhi, K.S. Nanjundaswamy, J.B. Goodenough, Journal of the Electrochemical Society 144 (1997) 1188–1194.
[20] J. Arai, T. Yamaki, S. Yamauchi, T. Yuasa, T. Maeshima, T. Sakai, M. Koseki, T. Horiba, Journal of Power Sources 146 (2005) 788–792.
[21] C. Delacourt, L. Laffont, R. Bouchet, C. Wurm, J.B. Leriche, M. Morcrette, J.M. Tarascon, C. Masquelier, Journal of the Electrochemical Society 152 (2005) A913–A921.
[22] W. Ojczyk, J. Marzec, K. Swierczek, W. Zajac, M. Molenda, R. Dziembaj, J. Molenda, Journal of Power Sources 173 (2007) 700–706.
[23] D. Morgan, A. Van der Ven, G. Ceder, Electrochemical and Solid State Letters 7 (2004) A30–A32.
[24] F. Sauvage, E. Baudrin, L. Gengembre, J.M. Tarascon, Solid State Ionics 176 (2005) 1869–1876.
[25] K.F. Chiu, P.Y. Chen, Surface & Coatings Technology 203 (2008) 872–875.
[26] Z.G. Lu, M.F. Lo, C.Y. Chung, Journal of Physical Chemistry C 112 (2008) 7069–7078.
[27] Y.Y. Liu, D.W. Liu, Q.F. Zhang, D.M. Yu, J. Liu, G.Z. Cao, Electrochimica Acta 56 (2011) 2559–2565.
[28] K. Saravanan, M.V. Reddy, P. Balaya, H. Gong, B.V.R. Chowdari, J.J. Vittal, Journal of Materials Chemistry 19 (2009) 605–610.
[29] V. Palomares, I.R. de Larramendi, J. Alonso, M. Bengoechea, A. Goni, O. Miguel, T. Rojo, Applied Surface Science 256 (2010) 2563–2568.
[30] J. Xie, N. Imanishi, T. Zhang, A. Hirano, Y. Takeda, Y. Yamamoto, Journal of Power Sources 192 (2009) 689–692.
[31] K. Saravanan, P. Balaya, M.V. Reddy, B.V.R. Chowdari, J.J. Vittal, Energy & Environmental Science 3 (2010) 457–464.
[32] A.A. Deshmukh, S.D. Mhlanga, N.J. Coville, Materials Science & Engineering R-Reports 70 (2010) 1–28.
[33] J.D. Wilcox, M.M. Doeff, M. Marcinek, R. Kostecki, Journal of the Electrochemical Society 154 (2007) A389–A395.
[34] D.W. Liu, Y.H. Zhang, P. Xiao, B.B. Garcia, Q.F. Zhang, X.Y. Zhou, Y.H. Jeong, G.Z. Cao, Electrochimica Acta 54 (2009) 6816–6820.
[35] X.D. Yan, G.L. Yang, J. Liu, Y.C. Ge, H.M. Xie, X.M. Pan, R.S. Wang, Electrochimica Acta 54 (2009) 5770–5774.
[36] X.H. Wang, J.G. Li, H. Kamiyama, M. Katada, N. Ohashi, Y. Moriyoshi, T. Ishigaki, Journal of the American Chemical Society 127 (2005) 10982–10990.
[37] H.M. Liu, W.S. Yang, Y. Ma, Y. Cao, J.N. Yao, New Journal of Chemistry 26 (2002) 975–977.
[38] M.M. Doeff, J.D. Wilcox, R. Yu, A. Aumentado, M. Marcinek, R. Kostecki, Journal of Solid State Electrochemistry 12 (2008) 995–1001.
[39] D.W. Liu, Y.Y. Liu, B.B. Garcia, Q.F. Zhang, A.Q. Pan, Y.H. Jeong, G.Z. Cao, Journal of Materials Chemistry 19 (2009) 8789–8795.
[40] X.L. Wu, L.Y. Jiang, F.F. Cao, Y.G. Guo, L.J. Wan, Advanced Materials 21 (2009) 2710–2714.
[41] Y.Z. Dong, Y.M. Zhao, Y.H. Chen, Z.F. He, Q. Kuang, Materials Chemistry and Physics 115 (2009) 245–250.
[42] K. Dokko, S. Koizumi, H. Nakano, K. Kanamura, Journal of Materials Chemistry 17 (2007) 4803–4810.
[43] T. Maxisch, F. Zhou, G. Ceder, Physical Review B 73 (2006) 104301.
[44] M.S. Islam, D.J. Driscoll, C.A.J. Fisher, P.R. Slater, Chemistry of Materials 17 (2005) 5085–5092.
[45] K.F. Chiu, C.L. Chen, Surface & Coatings Technology 205 (2010) 1642–1646.
[46] H. Yang, X.L. Wu, M.H. Cao, Y.G. Guo, Journal of Physical Chemistry C 113 (2009) 3345–3351.
[47] N. Meethong, H.Y.S. Huang, W.C. Carter, Y.M. Chiang, Electrochemical and Solid State Letters 10 (2007) A134–A138.
[48] P. Gibot, M. Casas-Cabanas, L. Laffont, S. Levasseur, P. Carlach, S. Hamelet, J.M. Tarascon, C. Masquelier, Nature Materials 7 (2008) 741–747.
[49] J. Maier, Nature Materials 4 (2005) 805–815.
[50] M. Winter, R.J. Brodd, Chemical Reviews 105 (2005) 1021.
[51] J. Wang, J. Polleux, J. Lim, B. Dunn, Journal of Physical Chemistry C 111 (2007) 14925–14931.
[52] H. Zhang, G.R. Li, L.P. An, T.Y. Yan, X.P. Gao, H.Y. Zhu, Journal of Physical Chemistry C 111 (2007) 6143–6148.
[53] J.Y. Luo, Y.G. Wang, H.M. Xiong, Y.Y. Xia, Chemistry of Materials 19 (2007) 4791–4795.
[54] S. Adams, Applied Energy 90 (2012) 323–328.